Supplementary Information

Crown ether functionalized large-area graphene oxide and MXene hybridize as ion-sieving layers for high-performance lithium-sulfur batteries

Yun-Sheng Ye*[a‡], Mohamed Gamal Mohamed[a,b‡], Meng-Che Tsai[c], Huan-Yu Hu[a], Bing-Joe Hwang[d] and Shaw-Wei Kuo*[a]

a. Department of Materials and Optoelectronic Science, Center of Crystal Research, National Sun Yat-Sen University, Kaohsiung, 80424, Taiwan.

b. Chemistry Department, Faculty of Science, Assiut University, Assiut 71515, Egypt.

c. Department of Greenergy, National University of Tainan, Tainan 700301, Taiwan.

d. Department of Chemical Engineering, National Taiwan University of Science and Technology, Taipei106335, Taiwan.

‡. Contributed equally.

S1. Materials

The MAX-Ti_3AlC_2 (≥ 98 %) was purchased from 11 Tech Company, lithium fluoride (LiF, ≥ 99.9 %), graphite (powder, <20 μm, synthetic), potassium permanganate ($KMnO_4$, ≥ 99.0 %), di(2-chloroethyl) ether (>99%), and 1,4-benzoquinone (>98%) was purchased from Sigma-Aldrich Company, lithium bis(trifluoromethanesulfonyl)imide (LiTFSI, ≥ 98 %), palladium on carbon (Pt/C, 5 wt.%), hydrogen peroxide (H_2O_2, 30 wt.%) and sublimed sulfur (analytical pure) were purchased from Adamas Company, HCl (36~38%), dimethylformamide (DMF, ≥ 99.5 %), tetrahydrofuran (THF, ≥ 99.8 %), dichloromethane (≥ 99.8 %, DCM), acetone (≥ 98 %) and anhydrous ethanol (≥ 99.7 %) were purchased from Thermo Fisher Scientific Co., Ltd., bisphenol (98 %), sodium hydroxide (NaOH, 98 %), lithium nitrate ($LiNO_3$, 99 %), acetic acid (36 wt.%) and lithium hydrosulfide (Li_2S, 99.5 %) were purchased from LeYan Company, Li sheets (battery level, 1 mm thick) , polyvinylidene difluoride (PVDF, HSV900 type), conductive carbon black (analytical pure) and aluminum foil (≥ 99.7 %, 15 μm thick) were purchased from Shenzhen Kaishenzhi Technology Co., Ltd. The above drugs, reagents do not require further purification and can be used directly. 1,3-dioxolane (DOL, 98 %) and 1,2-dimethoxyethane (DME, 99 %) were purchased from TCI Company, N-methyl pyrrolidone (NMP, ≥ 99.9 %) was purchased from TCI Co., Ltd., and must be distilled and dried before use. Polyethylene membrane (PE, thickness 16 μm) was purchased from Alfa Chemistry Co., Ltd.

S2. Experimental

S2.1. Synthesis route for DB18C6-2NH$_2$[S1]

Scheme S1 featured schematic representations of the procedures associated with the synthesis of di(aminobenzo)[18]crown-6 (DB18C6).

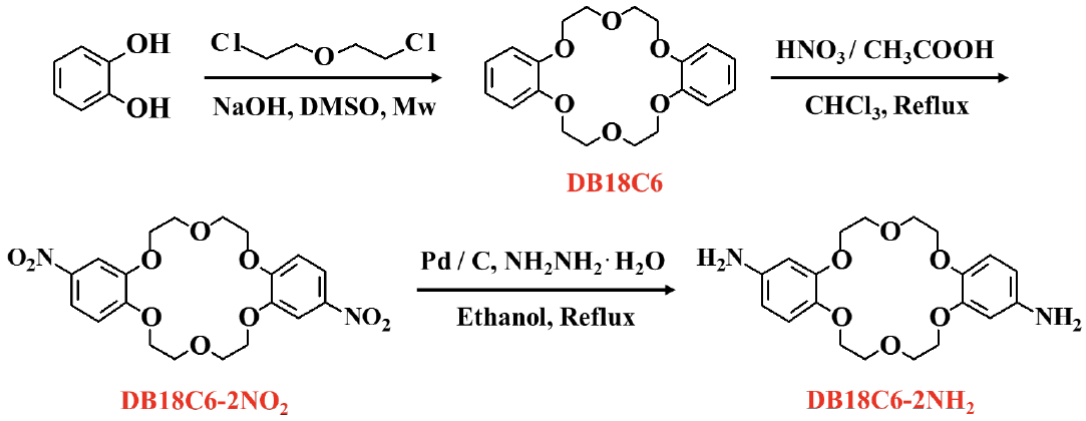

Scheme S1. Schematic illustrations for synthesis processes of DB18C6-2NH$_2$.

Synthesis of dibenzo-18-crown-6 (DB18C6): 2.20 g of bisphenol, 2.24 g of sodium hydroxide, and 2.86 g of di(2-chloroethyl) ether were dissolved in 15 mL of anhydrous DMF and stir at 70 °C for 4 h. The mixture was dissolved into a mixed solution of 300 mL of ice water and 10 mL of HCl (36-38 wt.%) and stir at 25 °C for 2 h. The solution was extracted twice using DCM. Collect the organic layer, dehydrate using anhydrous $MgSO_4$, and then filter. The organic solution was evaporated using a rotary evaporator, resulting in a solid powder. This powder was then washed with 100 mL of acetone and dried under vacuum at 50 °C for 24 hours to produce fibrous needle shaped DB18C6.

^{1}H NMR (600 MHz, DMSO): δ = 6.94 (d, 4H), 6.85 (d, 4H), 4.06 ~ 3.87 (m, 8H), 3.86 ~ 3.71 (m, 8H).

Synthesis of dibenzo-18-crown-6-2-nitro (DB18C6-2NO$_2$): 3.00 g of dibenzo-18-crown-6 was dissolved in a mixed solution of 80 mL of DCM and 10 mL of acetic acid (36 wt.%) and stir at room temperature for 1 h. Then dropwise add a mixture of 5 mL of acetic acid and 2 mL of nitric acid at 50 °C and react for 24 h. After the reaction is complete, filter out the white solid, wash with methanol several times, and obtain DB18C6-2NO$_2$.

^{1}H NMR (600 MHz, DMSO): δ = 7.89 (dd, 2H), 7.73 (d, 2H), 7.16 (d, 2H), 4.24 (m, 8H), 3.90 ~ 3.83 (m, 8H).

Synthesis of dibenzo-18-crown-6-2-diamine (DB18C6-2NH$_2$): 5.00 g of dibenzo-18-crown-6-2-nitro, 0.05 g of Pd/C catalyst, 40 mL of dried 1,4-benzoquinone, and 20 mL of anhydrous ethanol were added to a flask, and heat at 100 °C under nitrogen atmosphere for 1 h. 10 mL of hydrazine hydrate was slowly added to the reaction mixture, and heat at 100 °C for 48 h. The mixture proceeded filtration to remove any residual Pd/C catalyst, and then evaporation of the solvent under reduced pressure to obtain the white powder DB18C6-2NH$_2$.

^{1}H NMR (600 MHz, DMSO): δ = 6.63 (d, 2H), 6.26 (d, 2H), 6.06 (dd, 2H), 4.54 (s, 4H), 4.00 ~ 3.92 (m, 8H),

3.84 ~ 3.76 (m, 8H).

S2.2. Synthesis of large-area graphene oxide (GO)[S2]

Synthesis of GO: GO nanosheets were synthesized using an enhanced Hummer technique. 3.0 g of graphite powder was added in a flask, followed by the addition of 70 mL of concentrated sulfuric acid and was stirred in an ice bath. Slowly add 9.0 g of $KMnO_4$ to the reaction system, and strictly control the reaction temperature below 20 °C. After the addition is complete, transfer the reaction system to a 40 °C oil-bath and stir for 12 h. The reaction mixture was cooled to room temperature and poured onto ice with 15 mL of H_2O_2 (30 wt.%) to continue the reaction until the solution color changes from brownish to yellow. After the reaction is finished, allow the reaction system to stand for 4 h, remove the top clear liquid, and rinse the solid with 250 mL of diluted HCl (1:10) three times to eliminate strong acids and metal ions. Then wash with deionized water and dilute the solid to 500 mL with ultrasonicate for 1 h to obtain GO suspension. After 24 h of suspension, the graphite and GO with insufficient dispersion were precipitated to the bottom of the container. Purify the supernatant using dialysis for one week to remove any residual impurity ions.

Filtration of large-area GO[S3]: Dilute the purified GO dispersion to 0.2 mg mL^{-1}, centrifuge at 1500 rpm for 30 min, separating large-area and small-area GO nanosheets which are collected at the bottom and top of the centrifuge tube, respectively. The GO is then collected at the bottom of the centrifuge tube, diluted, and centrifuged again under the same conditions. Repeat this process three times, and finally collect the filtered large-area GO from the bottom of the centrifuge tube, concentrating it to 10 mg mL^{-1} for the synthesis of CE-functionalized GO (GO-CE).

S2.3. Preparation of MXene nanosheets

The condensed formula for two-dimensional transition metal carbide/nitride (MXene) is $M_{n+1}X_nT_x$ (n = 1, 2, 3), where M denotes a transition metal like Ti, V; X represents C and/or N; T_x indicates surface terminal groups like as -O, -OH, and -F.[S4] Few-layer MXene is obtained by selectively etching the aluminum layer in the MAX-Ti_3AlC_2 precursor with HF, as shown in **Scheme S2**.

Preparation of multi-layer $Ti_3C_2T_x$ MXene: 1.0 g of LiF is added to a reaction flask containing 20 mL of HCl (36 ~ 38 wt.%), stirred at room temperature for 30 min to generate enough hydrofluoric acid. Then 1 g of MAX-Ti_3AlC_2 is slowly added to the above container and stirred continuously at 35 °C for 24 h. After the reaction is complete, the reaction mixture is centrifuged at 3500 rpm for 30 min, the upper layer of strong acidic liquid is discarded, and the sediment is diluted with DI water and ultrasonicated for 10 min. Then it is centrifuged at 3500 rpm for 30 min. The above steps are repeated until the pH of the upper layer is close to 6, and gray multi-layer $Ti_3C_2T_x$ MXene is obtained.

Preparation of few-layer MXene: The product after etching with HF acid is a concertina-shaped or multi-layer sheet, which can be easily exfoliated into single-layer or few-layer MXene sheets under the action of an intercalant. The specific method is: The purified $Ti_3C_2T_x$ MXene is removed and combined with ethanol

(intercalant) at a weight ratio of 1 : 200. Subsequently, the mixture is subjected to ultrasonication for 1 h. The mixture is centrifuged at 10000 rpm for 1 h, and the sediment is recovered to get black few-layer MXene. The MXene is concentrated to a concentration of 13.5 mg mL^{-1} for future usage.

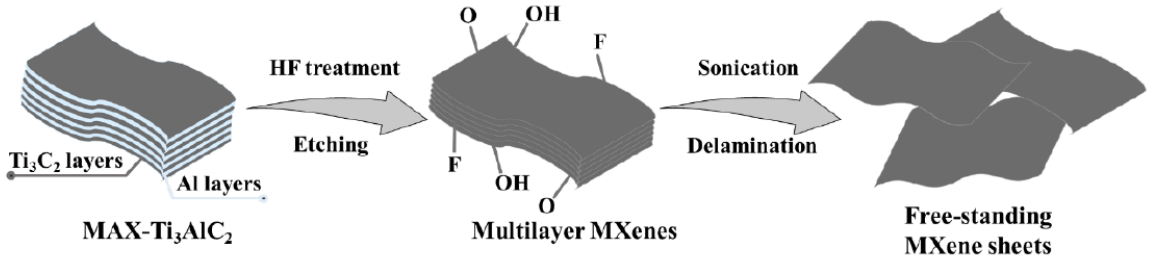

Scheme S2. Schematic illustrations of the fabrication process of MXene.

S2.4. Fabrication of S-cathode

The sulfur cathode is prepared by mixing elemental sulfur, conductive agent, and binder in a ratio of 6 : 3 : 1 by mass to form a coating slurry in NMP. Specifically, 0.8 g of binder (PVDF) is dissolved in 56 mL of anhydrous NMP, and 4.8 g of sublimed sulfur powder and 2.4 g of conductive carbon black are ground thoroughly in a mortar and pestle. The mixed powder is then added to the NMP solution and stirred with a magnetic stirrer for 1 h to obtain a preliminary mixed slurry. The slurry is transferred to an ARE-310 planetary centrifugal mixer and stirred at 1200 rpm for 30 min, followed by 2000 rpm for another 30 min to uniformly mix the high-viscosity slurry. The slurry is then coated onto Al foil using a coating machine, dried overnight at 70 °C, and then transferred to a vacuum oven at 60 °C for 8 h. The electrode sheets used in the electrochemical tests in this chapter have sulfur loading of approximately 1.5 and 4 mg cm^{-2}.

S2.5. Preparation of electrolyte for Li-S batteries

The Li-S battery electrolyte is prepared by mixing DOL and DME in a 1:1 volume ratio, and then adding 1 wt.% $LiNO_3$ and 1 M LiTFSI to the mixed solution. The solution is stirred with a magnetic stirrer for 30 min to ensure a uniform mixture. The electrolyte contains 20 μL of electrolyte per milligram of active material sulfur for each cell. The preparation is carried out in a glove box with high-purity nitrogen.

S2.6. Synthesis of Li_2S_6

Li_2S_6 in nominal stoichiometry, a representative of polysulfides, was synthesized by mixing sulfur and Li_2S at a molar ratio of 5:1 in a solvent of DOL : DME (1:1 in a volume ratio) followed by vigorous magnetic stirring for 24 h at 50 °C.

S3. Characterization

S3.1. ^1H NMR spectra were recorded on a Varian INOVA-400 MHz type (1H, 400 MHz) spectrometer. The samples were characterized by scanning electron microscopy (SEM) and energy-dispersive X-ray spectroscopy (EDX) elemental mapping (FEI Nova NanoSEM450). Transmission electron microscopy (TEM, JEOL JEM-1200CX-II). Thermogravimetric analysis (TGA, Q50) from room temperature to 800 °C at a

heating rate of 10 °C min^{-1} under N_2 atmosphere. The Fourier transform infrared spectroscopy (FTIR, Nicolet Avatar 320 FTIR spectrometer). The coating thickness was measured by a stylus profiler (DektakXT, Bruker). UV-visible spectra were measured by an Evolution 220. X-ray photoelectron spectroscopy (XPS, ESCA 2000 using a monochromatized Al Kα anode). The crystal structure was examined by the X-ray diffraction (XRD) pattern on a PAN alytical X'Pert PRO diffractometer equipped with Cu Kα radiation. The electrolyte contact angles were captured by an optical contact-angle measuring device (JC2000C1).

S3.2. Electrochemical properties

The cyclic voltammetry (*CV*) and electrochemical impedance spectroscopy (*EIS*) measurements were performed on an AUTO LAB impedance analyzer. The battery performance was measured by LAND Electronic Co., Ltd battery test system at 30 °C.

Electrolyte uptake (*EU*): To quantitatively evaluate the *EU* capacity of various separators, the separators are immersed in the electrolyte for a duration of 2 h. The *EU* is then calculated using the following equation (**Eq. S1**): $EU\ (\%) = (W_S - W_O) / W_O \times 100\%$, where W_S is the weight of the separator after soaking, and W_O is the weight of the dry separator before soaking. Before measuring the weight of the soaked separator, any excess electrolyte on the separator surface is removed using filter paper. To minimize experimental errors, three parallel tests are conducted simultaneously, and the mean value is used to determine the rate of *EU*.

Electrolyte retention (*ER*): *EU* is a crucial factor for assessing membrane performance and ensuring stability in Li-S batteries, alongside electrolyte absorption rate. After the electrolyte is fully saturated, the separator is placed in a 50 °C drier for 2 h. The separator's weight is measured every 2 min and obtained *ER* determined by following equation (**Eq. S2**): $ER\ (\%) = 100\% - (W_S - W_D)/W_S \times 100\%$, where W_D is the weight of the soaked separator after drying for specific period, and W_S is the weight of the soaked separator.

Ionic conductivity (σ): Ionic conductivity is measured through EIS and is calculated using the following equation (**Eq. S3**) : $\sigma = d / (S \times R_o)$, where d is the thickness of the separator, S is the area of the separator in the cell, and R_o is the intercept of the EIS curve with the horizontal axis, representing the ohmic resistance of the cell. Ionic conductivity is determined by assembling a test cell with 20 μL of electrolyte, which is left to stand for 2 h before testing. The testing frequency range is from 0.1 Hz to 5 MHz.

Li-ion diffusion coefficient (D_{Li^+}) is an important parameter for evaluating the Li-ion transport behavior and measuring the electrochemical kinetics of a separator. The diffusion coefficient can be calculated by measuring the CV curves at different scan rates and using the Randles-Sevcik equation (**Eq. S4**) : $I_p = 2.69 \times 10^5 n^{3/2} A C_{Li^+} \sqrt{D_{Li^+} \nu}$, where I_p is the peak current of the CV curve, n is the number of electron transfers in the electrochemical reaction ($n = 2$ for the conversion of S_8 to Li_2S_6 in Li-S batteries), A is the area of the electrode (ϕ = 12 mm, A = 1.13 cm^2), C_{Li^+} is the change in Li-ion concentration, and ν is the scan rate

of CV.

S3.3. Computational detail

The Vienna Ab initio Simulation Package (VASP) 5.4.4 code26 with the Perdew-Burke-Ernzerhof (PBE) functional performed all DFT calculations in the present work.[S5] The ion-electron interaction was described by the projector augmented wave (PAW) method[S6] with a cutoff energy of 500 eV. The DB18C6-coated graphite model with a 7×7 supercell was constructed to calculate the adsorption energy of lithium polysulfide (Li_2S_x). A *k*-point mesh with a size of 3×3×1 and the spin polarization was applied for the calculations. Furthermore, the DFT-D3 correction method in Grimme's scheme[S7] was used to accurately describe the long-range vdW interactions. All the calculations were carried out until the total energy and force were less than 10^{-5} eV per atom and 0.05 eV $Å^{-1}$, respectively. Finally, the adsorption energies (E_{ads}) were defined as follows:

$$E_{ads} = E_{ad/sub} - E_{sub} - E_{ad} \quad \textbf{Eq. S5}$$

where $E_{ad/sub}$, E_{ad}, and E_{sub} are the total energies of the optimized adsorbate (Li_2S_x)/substrate, the adsorbate in the gas phase, and the clean substrate (DB18C6-2NH_2/graphene, graphene), respectively. The free energies were acquired by $G = E_{total} + E_{ZPE} - TS$, where E_{total}, E_{ZPE}, and TS are the ground-state energy, zero-point energies, and entropy terms, respectively, with the latter two taking vibration frequencies from DFT calculations.

S3.4. Battery measurements

The CR2032 coin-type batteries were constructed by placing the pristine PE, GO, GO-CE, and MXene/GO-CE separators between the S-cathode and Li metal within an argon-filled glove box. The electrolyte contained 1 M LiTFSI and 1 wt.% $LiNO_3$ in the 1:1 vol ratio of DME/DOL. The electrolyte/sulfur (E/S) ratio was 10 μL mg^{-1}. All battery performances were measured in an oven at 30 °C.

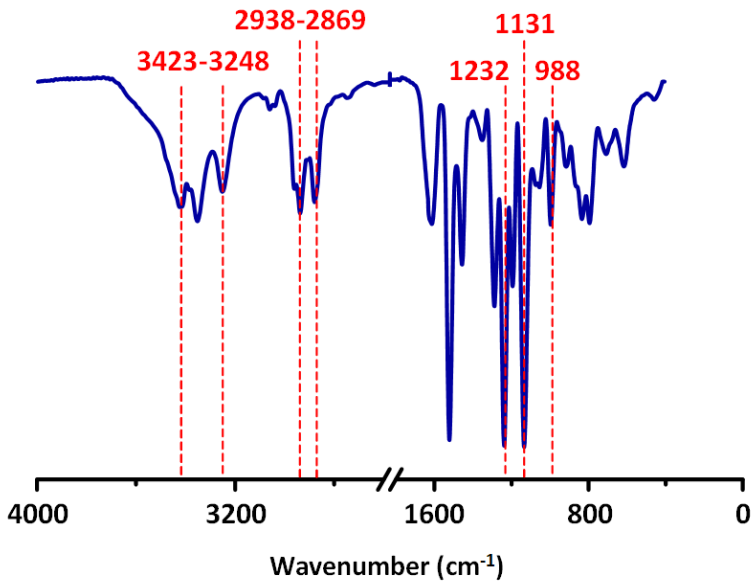

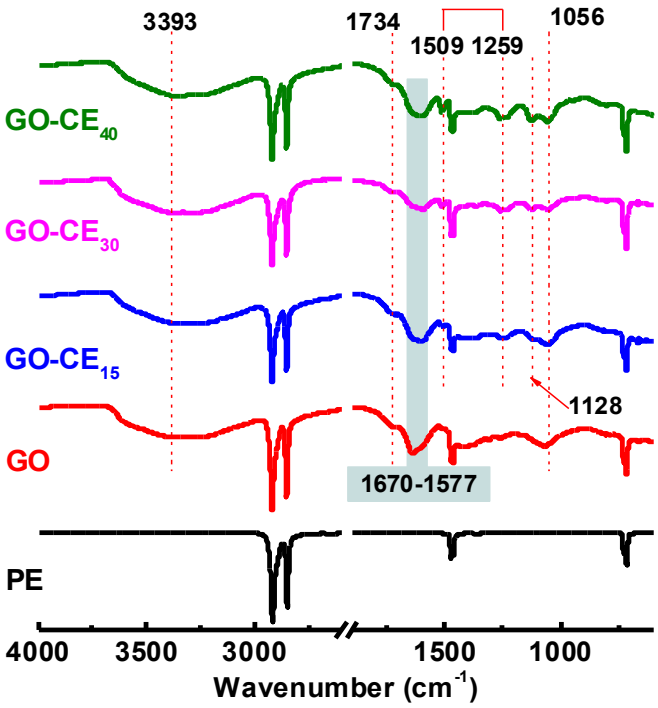

Figure S1. FTIR spectra of DB18C6-2NH_2, PE, GO, and GO-CE separators.

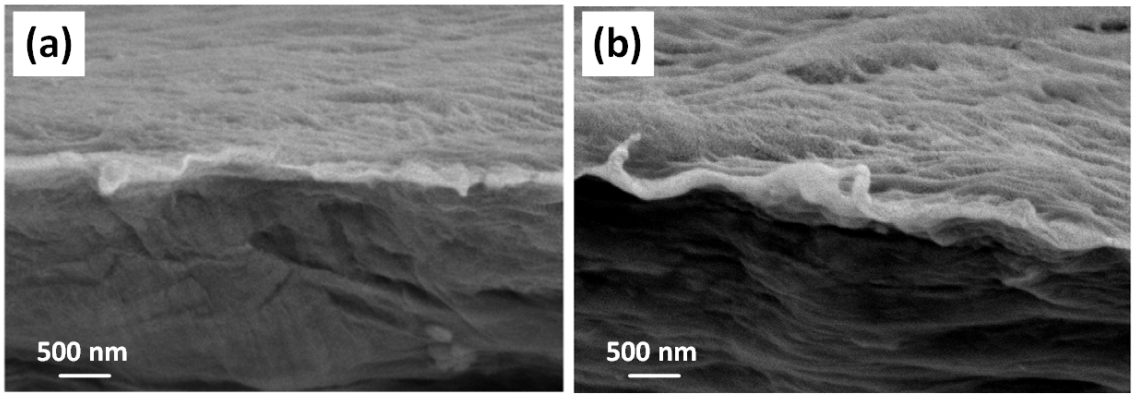

Figure S2. SEM images of (a) GO and (b) GO-CE_{30} modified separators.

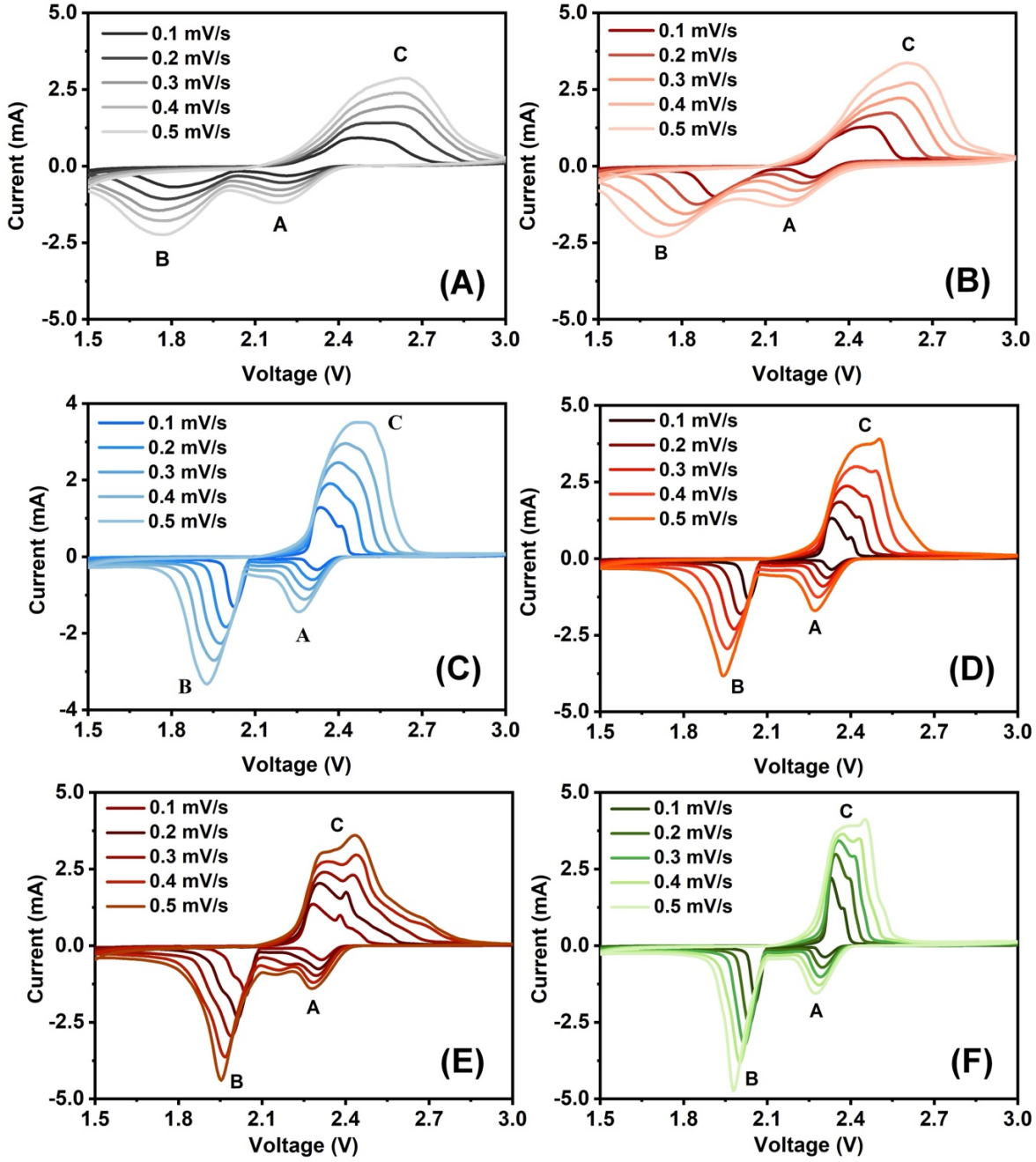

Figure S3. CV curves of cells with (A) PE, (B) GO, (C) GO-CE_{15}, (D) GO-CE_{30}, (E) GO-CE_{40}, and (F) MXene/GO-CE_{30} 4/1.

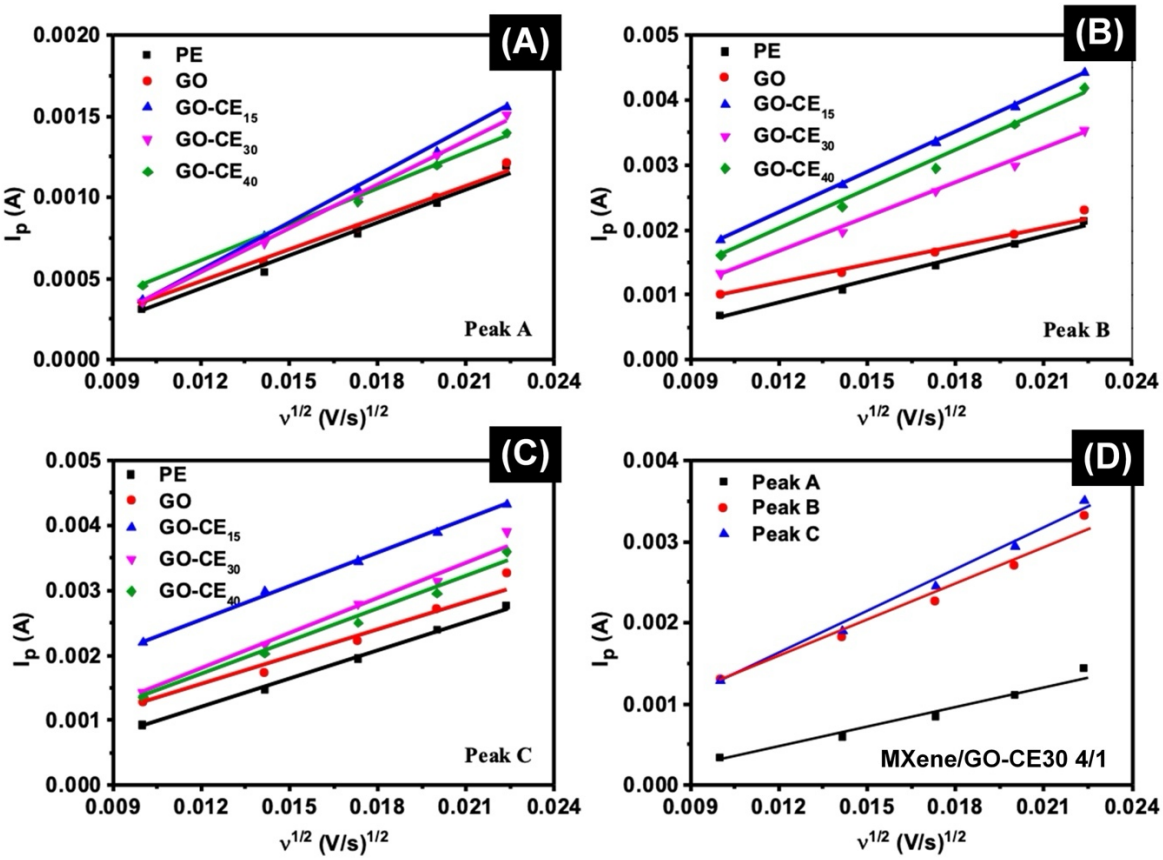

Figure S4. CV peak current (I_p) versus the square root of the scan rate ($v^{1/2}$) was analyzed in the voltage range of 1.5 - 3.0 V at different scan rates for peaks (A) A, (B) B, and (C) C in PE, GO, GO-CE, and (D) MXene/GO-CE_{30} 4/1.

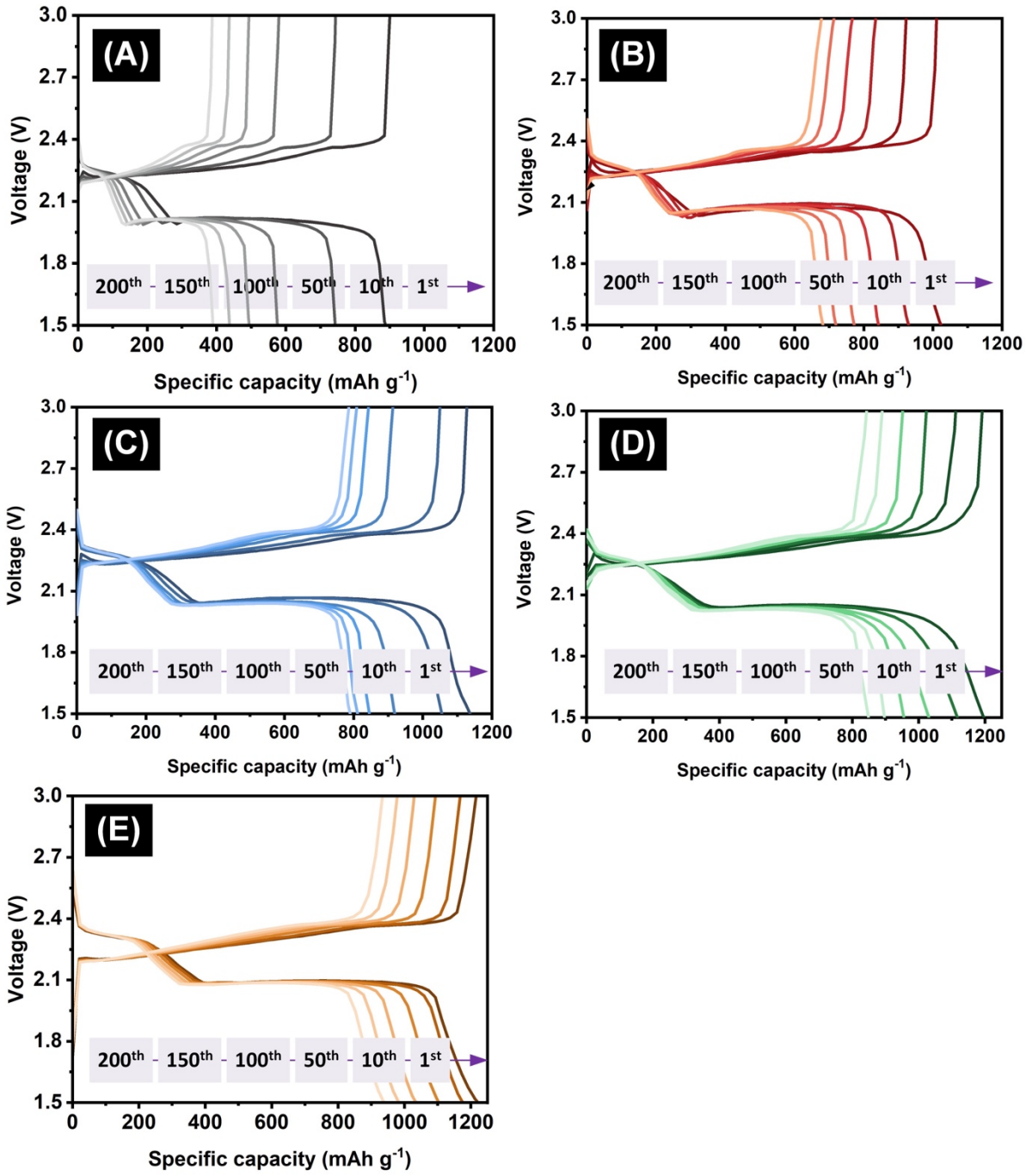

Figure S5. Charge-discharge profiles of the cells with (A) PE, (B) GO-CE_{30}, (C) MXene/GO-CE 2/3, (D) MXene/GO-CE 3/2, (E) MXene/GO-CE 4/1 separators.

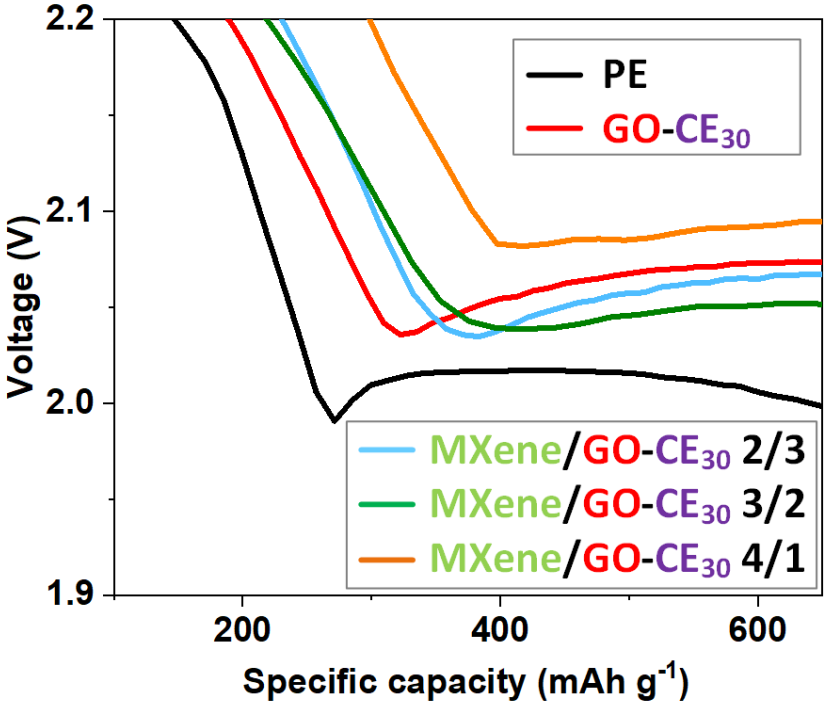

Figure S6. Overpotentials in the phase conversion between soluble Li_2S_4 and insoluble Li_2S_2/Li_2S.

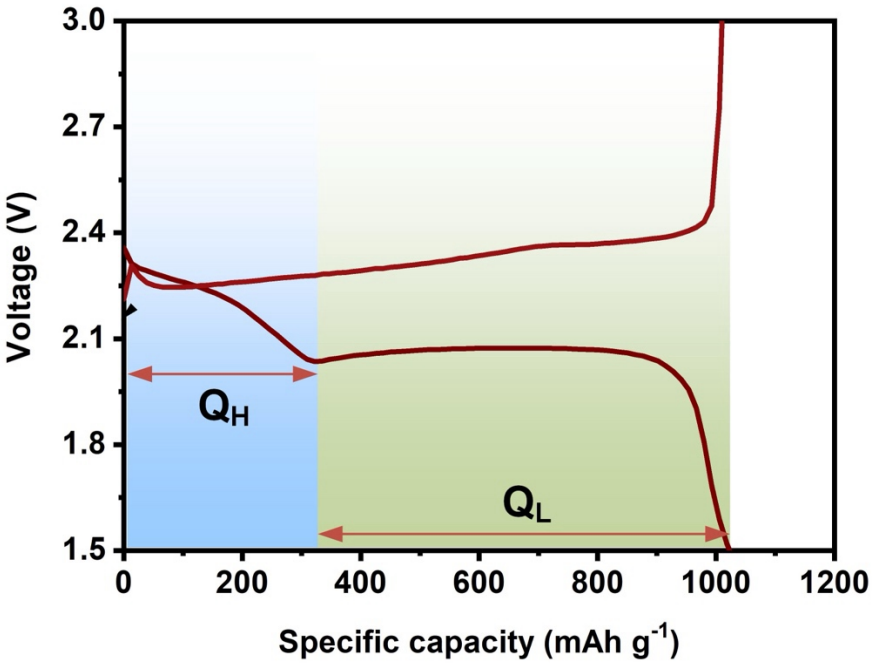

Figure S7. Illustrate the initial charge-discharge profile of cell with GO-CE_{30} modified separators by showing the higher- (Q_H) and lower-plateau discharge (Q_L).

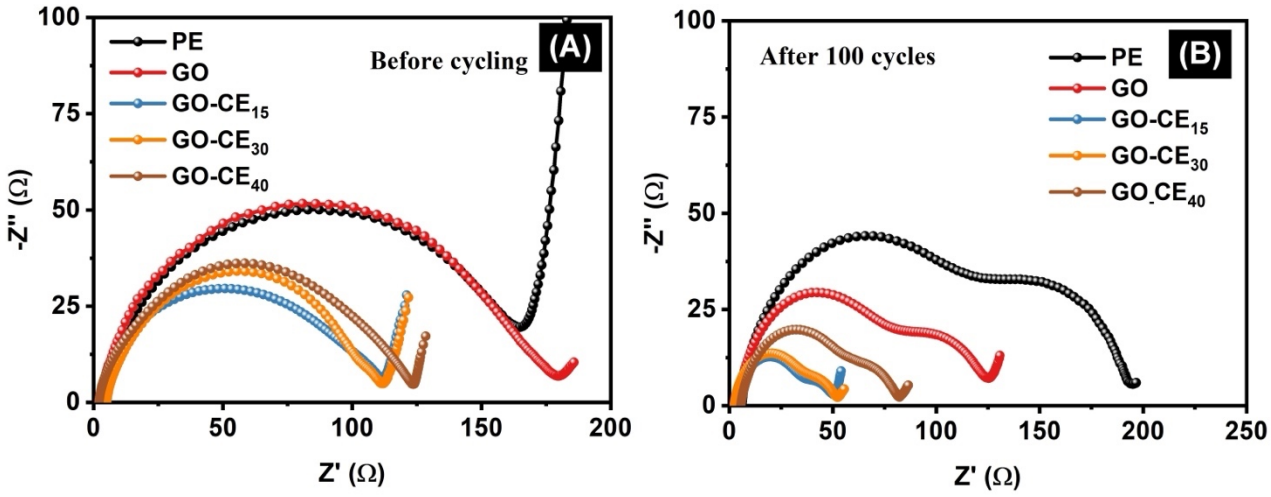

Figure S8. EIS of the cells with PE, GO and GO-CE modified separators.

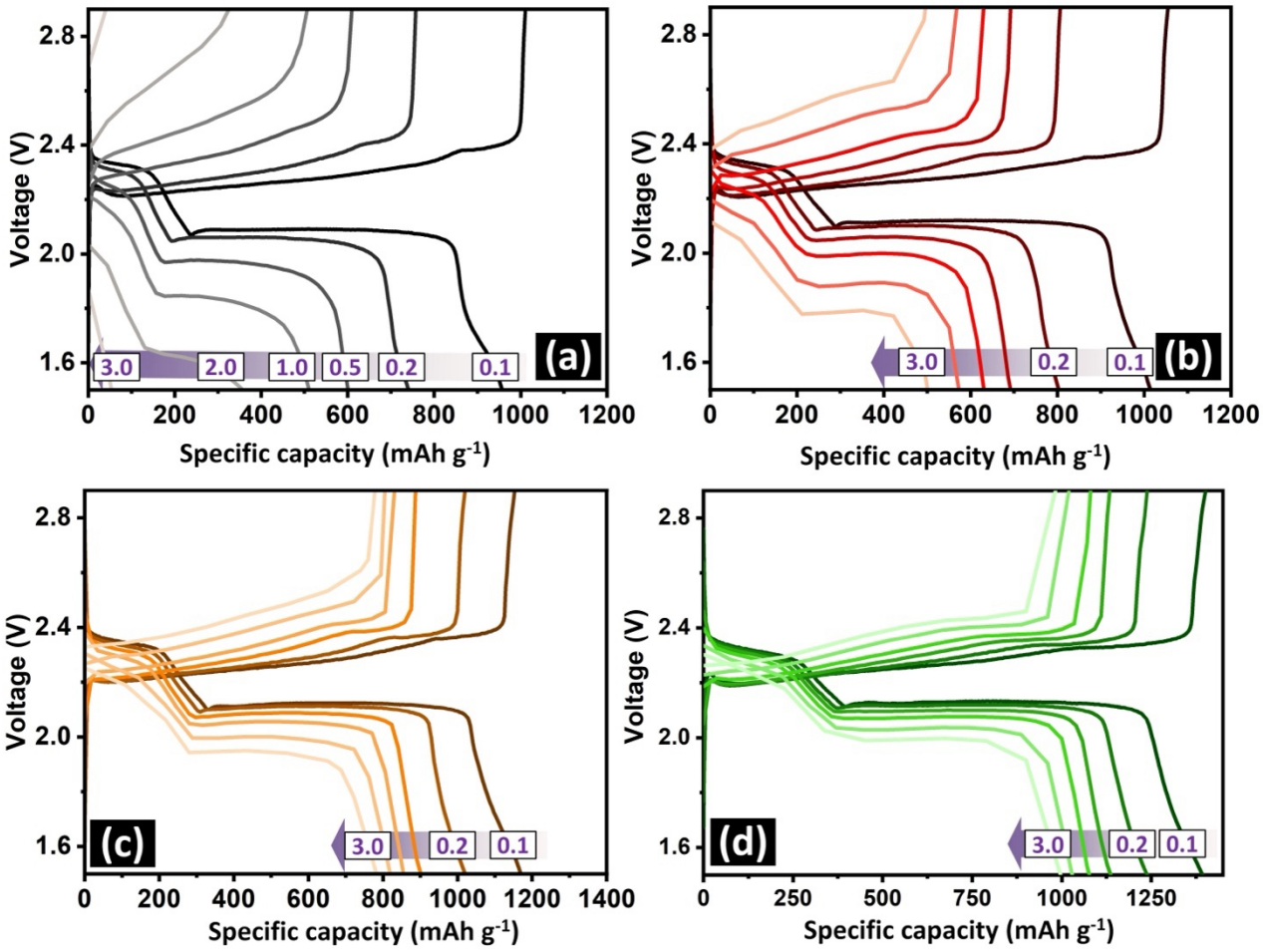

Figure S9. Charge/discharge profiles of cells with (a) PE, (b) GO, (c) GO-CE_{30}, and (d) MXene/GO-CE_{30} 4/1 separators.

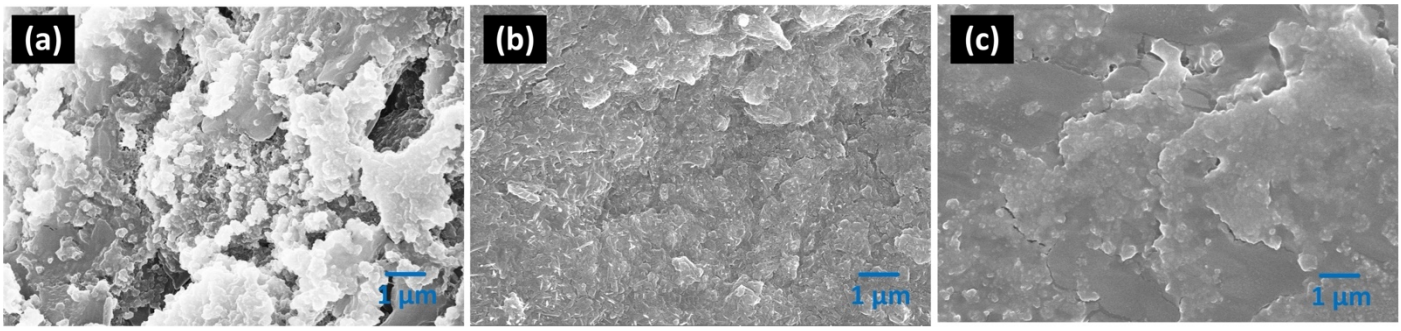

Figure S10. SEM images of Li metal surface from cycled cells with (a) PE, (b) GO-CE_{30}, and (c) MXene/GO-CE_{30} 4/1.

Table S1. Elemental analysis of GO and GO-CE.

Samples	Element content (wt.%)				Theoretical CE ratio (wt.%)	Calculated CE ratio (wt.%)
	C	H	O	N		
GO	49.2	3.0	44.1	-	-	-
GO-CE_{15}	52.1	3.2	39.1	1.0	15	14.5
GO-CE_{30}	54.3	3.1	36.4	1.9	30	27.5
GO-CE_{40}	55.6	3.4	33.1	2.5	40	36.2

Table S2. Summary of Ohmic resistance and ionic liquid conductivity of different separators.

Sample	R_o (Ω)	σ (mS cm^{-1})
PE	7.81	0.10
GO-CE_{30}	7.55	0.13
MXene/GO-CE_{30} 2/3	6.39	0.15
MXene/GO-CE_{30} 3/2	5.97	0.16
MXene/GO-CE_{30} 4/1	3.36	0.28

Table S3. Summary of Li^+ diffusion coefficients of Li-S cells with different separators.

Sample	D_{Li^+} at peak A ($cm^2\ s^{-1}$)	D_{Li^+} at peak B ($cm^2\ s^{-1}$)	D_{Li^+} at peak C ($cm^2\ s^{-1}$)
PE	2.35×10^{-8}	6.36×10^{-8}	1.17×10^{-7}
GO	2.16×10^{-8}	4.85×10^{-8}	1.07×10^{-7}
GO-CE_{15}	4.15×10^{-8}	2.02×10^{-7}	1.43×10^{-7}
GO-CE_{30}	3.98×10^{-8}	1.61×10^{-7}	1.51×10^{-7}
GO-CE_{40}	2.65×10^{-8}	2.01×10^{-7}	1.33×10^{-7}
MXene/GO-CE_{30} 4/1	3.52×10^{-8}	1.16×10^{-7}	1.47×10^{-7}

Table S4. Comparison of separator modified with GO/or rGO in Li-S batteries.

Modifier	Thickness /mass of modifier (μm /mg cm^{-2})	Method	binder	S-loading (mg cm^{-2})	Initial capacity (mAh g^{-1})	Decaying rate (%)	Cycles	Current (C)	Ref
MoS_2@CF-NrGO	10/-	Vacuum Assistant Filtration (VAF)	PVDF	1.0-1.2	≈1000	0.064	1000	1	S8
Li-MOF /rGO	1.2 /0.5-0.6			1.2-1.4	≈1480[a]	0.089	600	1	S9
MOF/rGO					≈1280[a]	0.103			
Nb_2O_5/rGO	20 /0.1-0.5			1.5	≈1100	0.086	500	≈0.3	S10
CeO_2@G	25/0.38			1.2	1039	0.12	200	0.5	S11
FM@G/MoS_2	12.5/0.3			Li_2S_6 solution (0.5 M)	1040	0.08	300	1	S12
rGO/MoS_2/C	-/-			1.5	~1400[a]	0.002	1000	2	S13
SrF_2/graphene	22/0.6		PTFE	-	1140	0.05	350	0.5	S14
$WN_{0.67}$@NG	5.6/0.3		LA132	1.2-1.5	≈900	0.045	800	1	S15
Ni_3Sn_2/NG	-/0.4		LA133	1.6	1022	0.07	400	1	S16
rGO@MoS_2	≈8/0.24		NO	1.8-2.0	877	0.116	500	1	S17
Nb_2O_5-rGO	0.2/0.05			1	~680[a]	0.08	500	3	S18
CoPc@GO	0.2/0.022			2.5	1092	0.08	400	1	S19
PNCG	24/0.35	Blade Coating	PVDF	Li_2S_6 solution (0.25 M)	1192	0.05	800	0.1	S20

CaF_2@rGO	14/-			-	1005	0.06	420	0.5	S21
W/NG	13/0.32			1.1	1100	0.05	100	2	S22
Sb_2Se_3/rGO	32/0.5			1.8	945	0.03	500	1	S23
Ni_3B@rGO	23/~0.23			1.5	572	0.06	500	2	S24
Co-3DC-rGO	20/-			1.5	~1300[a]	0.12	500	1	S25
ZnS-RGA	8/0.1			1.5	800	0.1	500	1	S26
Ni@C/G	-/≈0.4			2.0	1337.4	0.061	1000	0.5	S27
$LiNiPO_4$/rGO	20/0.88		LA133	1.5	945	0.02	1400	1.5	S28
GO-CE_{30}	~0.1/0.06		No	1.5		0.035	1500	1	This work
MXene/GO-CE_{30} 4/1						0.025			

[a] Value determined by reading of the data in the article.

Abbreviation

MoS_2@CF-NrGO: nitrogen-doped rGO and carbonized melamine foam; *Li-MOF/rGO*: Li-ion inserted ZIF-67 and rGO; *Nb_2O_5/rGO*: heterostructural Nb_2O_5 nanocrystals/rGO; *$WN_{0.67}$NG*: $WN_{0.67}$-embedded N-doped graphene nanosheets; *FM@G*: sulfur-deficient metallic 1T-MoS_2 nanoflowers decorated graphene; *CoPc@GO*: GO loaded with Co phthalocyanine; *PCNG*: g-C_3N_4/carbon heterostructure on graphene nanosheet; *Ni_3Sn_2/NG*: Ni_3Sn_2/nitrogen-doped graphene; *W/NG*: tungsten single-atom catalyst immobilized on nitrogen-doped graphene; *CeO_2@G*: CeO_2 decorated graphene; *CaF_2@rGO*: rGO embedded with nano-calcium fluoride particles; *SrF_2/graphene*: strontium fluoride graphene sandwich; *Sb_2Se/rGO*: defect-rich Sb_2Se_3−x nanorods wrapped by rGO; *Co-3DC-rGO*: cobalt metal nanoparticles/three-dimensional carbon/rGO; *ZnS-RGA*: zinc sulfide quantum dots/rGO aerogel; *Ni@C/G*: dispersing graphene-supported Ni nanoparticles with carbon coating

Reference

(1) Mohamed, M. G.; Kuo, S.-W. Crown Ether-Functionalized Polybenzoxazine for Metal Ion Adsorption. *Macromolecules* **2020**, *53* (7), 2420-2429. DOI: 10.1021/acs.macromol.9b02519.

(2) Marcano, D. C.; Kosynkin, D. V.; Berlin, J. M.; Sinitskii, A.; Sun, Z.; Slesarev, A.; Alemany, L. B.; Lu, W.; Tour, J. M. Improved Synthesis of Graphene Oxide. *ACS Nano* **2010**, *4* (8), 4806-4814. DOI: 10.1021/nn1006368.

(3) Wang, X.; Bai, H.; Shi, G. Size Fractionation of Graphene Oxide Sheets by pH-Assisted Selective Sedimentation. *Journal of the American Chemical Society* **2011**, *133* (16), 6338-6342. DOI: 10.1021/ja200218y.

(4) Murali, G.; Reddy Modigunta, J. K.; Park, Y. H.; Lee, J.-H.; Rawal, J.; Lee, S.-Y.; In, I.; Park, S.-J. A Review on MXene Synthesis, Stability, and Photocatalytic Applications. *ACS Nano* **2022**, *16* (9), 13370-13429. DOI: 10.1021/acsnano.2c04750.
(5) Perdew, J.; Burke, K.; Ernzerhof, M. of Physics, D.; Quantum Theory Group Tulane University, NOL 70118 J. *Phys. Rev. Lett* **1996**, *77* (18), 3865-3868.
(6) Kresse, G.; Joubert, D. From ultrasoft pseudopotentials to the projector augmented-wave method. *Physical review b* **1999**, *59* (3), 1758.
(7) Grimme, S.; Antony, J.; Ehrlich, S.; Krieg, H. A consistent and accurate ab initio parametrization of density functional dispersion correction (DFT-D) for the 94 elements H-Pu. *The Journal of chemical physics* **2010**, *132* (15), 154104. Grimme, S.; Ehrlich, S.; Goerigk, L. Effect of the damping function in dispersion corrected density functional theory. *Journal of computational chemistry* **2011**, *32* (7), 1456-1465.
(8) Zhang, J.; Xu, G.; Zhang, Q.; Li, X.; Yang, Y.; Yang, L.; Huang, J.; Zhou, G. Mo-O-C Between MoS2 and Graphene Toward Accelerated Polysulfide Catalytic Conversion for Advanced Lithium-Sulfur Batteries. *Advanced Science* **2022**, *9* (22), 2201579. DOI: https://doi.org/10.1002/advs.202201579.
(9) Zhou, M.; Li, Y.; Lei, T.; Chen, W.; Rao, G.; Xue, L.; Hu, A.; Fan, Y.; Huang, J.; Hu, Y.; et al. Ion-Inserted Metal–Organic Frameworks Accelerate the Mass Transfer Kinetics in Lithium–Sulfur Batteries. *Small* **2021**, *17* (44), 2104367. DOI: https://doi.org/10.1002/smll.202104367.
(10) Guo, P.; Sun, K.; Shang, X.; Liu, D.; Wang, Y.; Liu, Q.; Fu, Y.; He, D. Nb2O5/RGO Nanocomposite Modified Separators with Robust Polysulfide Traps and Catalytic Centers for Boosting Performance of Lithium–Sulfur Batteries. *Small* **2019**, *15* (40), 1902363. DOI: https://doi.org/10.1002/smll.201902363.
(11) Cheng, P.; Guo, P.; Sun, K.; Zhao, Y.; Liu, D.; He, D. CeO2 decorated graphene as separator modification material for capture and boost conversion of polysulfide in lithium-sulfur batteries. *Journal of Membrane Science* **2021**, *619*, 118780. DOI: https://doi.org/10.1016/j.memsci.2020.118780.
(12) Cheng, Z.; Chen, Y.; Yang, Y.; Zhang, L.; Pan, H.; Fan, X.; Xiang, S.; Zhang, Z. Metallic MoS2 Nanoflowers Decorated Graphene Nanosheet Catalytically Boosts the Volumetric Capacity and Cycle Life of Lithium–Sulfur Batteries. *Advanced Energy Materials* **2021**, *11* (12), 2003718. DOI: https://doi.org/10.1002/aenm.202003718.
(13) Fan, B.; He, Q.; Wei, Q.; Liu, W.; Zhou, B.; Zou, Y. Anchoring and catalyzing polysulfides by rGO/MoS2/C modified separator in lithium–sulfur batteries. *Carbon* **2023**, *214*, 118361. DOI: https://doi.org/10.1016/j.carbon.2023.118361.
(14) Jing, W.; Zu, J.; Zou, K.; Dai, X.; Song, Y.; Han, J.; Sun, J.; Tan, Q.; Chen, Y.; Liu, Y. Sandwich-like strontium fluoride graphene-modified separator inhibits polysulfide shuttling and lithium dendrite growth in lithium–sulfur batteries. *Journal of Materials Chemistry A* **2022**, *10* (9), 4833-4844, 10.1039/D2TA00002D. DOI: 10.1039/D2TA00002D.
(15) Ma, F.; Yu, B.; Zhang, X.; Zhang, Z.; Srinivas, K.; Wang, X.; Liu, D.; Wang, B.; Zhang, W.; Wu, Q.; Chen, Y. WN0.67-Embedded N-doped Graphene-Nanosheet Interlayer as efficient polysulfide catalyst and absorbant for High-Performance Lithium-Sulfur batteries. *Chemical Engineering Journal* **2022**, *431*, 133439. DOI: https://doi.org/10.1016/j.cej.2021.133439.
(16) Qi, X.; Huang, L.; Luo, Y.; Chen, Q.; Chen, Y. Ni3Sn2/nitrogen-doped graphene composite with chemisorption and electrocatalysis as advanced separator modifying material for lithium sulfur batteries. *Journal of Colloid and Interface Science* **2022**, *628*, 896-910. DOI: https://doi.org/10.1016/j.jcis.2022.08.031.
(17) Tan, L.; Li, X.; Wang, Z.; Guo, H.; Wang, J. Lightweight Reduced Graphene Oxide@MoS2 Interlayer

as Polysulfide Barrier for High-Performance Lithium–Sulfur Batteries. *ACS Appl Mater Interfaces* **2018**, *10* (4), 3707-3713. DOI: 10.1021/acsami.7b18645.
(18) Ma, Q.; Hu, M.; Yuan, Y.; Pan, Y.; Chen, M.; Zhang, Y.; Long, D. Colloidal dispersion of Nb(2)O(5)/reduced graphene oxide nanocomposites as functional coating layer for polysulfide shuttle suppression and lithium anode protection of Li-S battery. *J Colloid Interface Sci* **2020**, *566*, 11-20. DOI: 10.1016/j.jcis.2020.01.066 From NLM PubMed-not-MEDLINE.
(19) Shen, C.; Li, Y.; Gong, M.; Zhou, C.; An, Q.; Xu, X.; Mai, L. Ultrathin Cobalt Phthalocyanine@Graphene Oxide Layer-Modified Separator for Stable Lithium–Sulfur Batteries. *ACS Applied Materials & Interfaces* **2021**, *13* (50), 60046-60053. DOI: 10.1021/acsami.1c19859.
(20) Zhang, H.; Liu, Q.; Ruan, S.; Ma, C.; Jia, X.; Qiao, W.; Ling, L.; Wang, J. In-situ construction of g-C3N4/carbon heterostructure on graphene nanosheet: An efficient polysulfide barrier for advanced lithium-sulfur batteries. *Applied Surface Science* **2022**, *578*, 152022. DOI: https://doi.org/10.1016/j.apsusc.2021.152022.
(21) Jing, W.; Zou, K.; Dai, X.; Shi, M.; Sun, J.; Zhu, D.; Guo, S.; Chen, Y.; Liu, Y. A calcium fluoride composite reduction graphene oxide functional separator for lithium-sulfur batteries to inhibit polysulfide shuttling and mitigate lithium dendrites. *Journal of Colloid and Interface Science* **2021**, *601*, 305-316. DOI: https://doi.org/10.1016/j.jcis.2021.05.083.
(22) Wang, P.; Xi, B.; Zhang, Z.; Huang, M.; Feng, J.; Xiong, S. Atomic Tungsten on Graphene with Unique Coordination Enabling Kinetically Boosted Lithium–Sulfur Batteries. *Angewandte Chemie International Edition* **2021**, *60* (28), 15563-15571. DOI: https://doi.org/10.1002/anie.202104053.
(23) Tian, Y.; Li, G.; Zhang, Y.; Luo, D.; Wang, X.; Zhao, Y.; Liu, H.; Ji, P.; Du, X.; Li, J.; Chen, Z. Low-Bandgap Se-Deficient Antimony Selenide as a Multifunctional Polysulfide Barrier toward High-Performance Lithium–Sulfur Batteries. *Advanced Materials* **2020**, *32* (4), 1904876. DOI: https://doi.org/10.1002/adma.201904876.
(24) Shrshr, A. E.; Dong, Y.; Al-Tahan, M. A.; Kang, X.; Guan, H.; Zheng, X.; Zhang, J. Modified separator engineering with 2D ultrathin Ni3B@rGO: Extraordinary electrochemical performance of the lithium-sulfur battery with enormous-sulfur-content cathode in low electrolyte/sulfur ratio. *Journal of Alloys and Compounds* **2022**, *910*, 164917. DOI: https://doi.org/10.1016/j.jallcom.2022.164917.
(25) Xiao, T.; Chen, Q.; Zhong, W.; Yang, M.; Cai, F.; Liu, W.; Ren, M.; Wang, Y. Cobalt/three-dimensional carbon/reduced graphene oxide modified PP separator for Li-S batteries. *Journal of Alloys and Compounds* **2022**, *907*. DOI: 10.1016/j.jallcom.2022.164486.
(26) Liu, Z.; Hu, Z.; Jiang, X.; Zhang, Y.; Wang, X.; Zhang, S. Multi-functional ZnS quantum Dots/Graphene aerogel modified separator for high performance lithium-sulfur batteries. *Electrochim Acta* **2022**, *422*, 140496. DOI: https://doi.org/10.1016/j.electacta.2022.140496.
(27) Yu, Z.; Wang, B.; Liao, X.; Zhao, K.; Yang, Z.; Xia, F.; Sun, C.; Wang, Z.; Fan, C.; Zhang, J.; Wang, Y. Boosting Polysulfide Redox Kinetics by Graphene-Supported Ni Nanoparticles with Carbon Coating. *Advanced Energy Materials* **2020**, *10* (25), 2000907. DOI: https://doi.org/10.1002/aenm.202000907.
(28) Zuo, Y.; Zhu, Y.; Wang, Q.; Lv, K.; Su, W.; Tang, Y.; Chen, Y. Promoting polysulfide conversion by catalytic separator with LiNiPO4 and rGO hybrids for high performance Li–S batteries. *Journal of Materials Chemistry A* **2020**, *8* (38), 20111-20121. DOI: 10.1039/d0ta07292c.